JOURNAL OF SOLID STATE CHEMISTRY 103, 63–74 (1993)

Structural Study of the Oxide $Pb_2Sr_2PrCeCu_3O_{10}$, Intergrowth of 0201- and 0222-Type Structures

T. ROUILLON, M. HERVIEU, B. DOMENGÈS, AND B. RAVEAU

Laboratoire CRISMAT, ISMRA/Université de Caen, Boulevard du Maréchal Juin, 14050 Caen Cedex, France

Received May 7, 1992; accepted August 4, 1992

The structure of the oxide $Pb_2Sr_2LnCeCu_3O_{10}$ was determined from powder X-ray and neutron diffraction data in the orthorhombic cell $a = 5.4522$ (2) Å, $b = 5.4807$ (2) Å and $c = 37.012$ (1) Å, space group *Fmmm*. This study is completed by an H.R.E.M. study. The structure consists of an intergrowth of 0201 and 0222 structures, i.e., it derives from the $Pb_2Sr_2YCu_3O_8$ structure by replacing one $[YO_2]_\infty$ simple fluorite layer by a $[Ln_2O_4]_\infty$ double fluorite layer. The main feature deals with the anionic disordering in the $[PbO]_\infty$ layers, leading to the tetrahedra PbO_3L, in which L characterizes the 6 s^2 lone pair of Pb(II). The twofold coordination of $Cu_{(1)}$ is also shown but no conclusion about the linearity of the Cu^1O_2 group can be drawn owing to the existence of a mirror plane at the level of $Cu_{(1)}$. The CuO_5 pyramids corresponding to $Cu_{(2)}$ exhibit a regular basal plane and the lanthanides are off center in the fluorite cages, having a 4 + 4 coordination. In spite of the existence of diffuse streaks and additional weak spots on the E.D. patterns, the H.R.E.M. images exhibit, for most of them, a very regular sequence in agreement with the N.D. and X.R.D. study; only some extended defects forming triple fluorite layers are observed in the bulk, whereas large fluorite domains appear on thin edges of the crystals.

Introduction

The possibility of introduction of additional fluorite-type layers in the cuprates was first demonstrated by the H.R.E.M. study of the oxides $TlBa_2NdCu_2O_7$ (*1*). The analysis of the structure of different layered cuprates (*2*), involving double pyramidal copper layers, showed that the cation located between the CuO_5 pyramids (calcium, yttrium, lanthanides) exhibits a pseudocubic coordination and forms a single fluorite-type layer. Such a close relationship suggested the possibility to intercalate, between pyramidal layers, double or triple fluorite-type layers. This view point was rapidly confirmed by the synthesis of the oxides $Tl_{1-x}A_{2-y}Ln_2Cu_2O_9$ (*3*) and $(Nd_{0.66}Sr_{0.20}Ce_{0.14})_2CuO_4$ (*4*, *5*). Afterwards, different new cuprates involving double fluorite-type layers were synthesized (*6–14*). Among these compounds, the oxides $Pb_2Sr_2LnCeCu_3O_{10+\delta}$ (*Ln* = Pr, Nd, Sm) were found to derive from the $Pb_2Sr_2YCu_3O_{8+\delta}$ structure (*15*, *17*) by introducing an additional fluorite layer. Only a structural model was established by X-ray diffraction; moreover this study was complicated by the existence of an excess oxygen δ. For this reason we have synthesized the stoichiometric phase $Pb_2Sr_2PrCeCu_3O_{10}$. We report here on its structure determina-

0022-4596/93 $5.00

tion by powder X-ray and neutron diffraction and on its high-resolution electron microscopy study.

Experimental

The reduced oxide was prepared from the oxides PbO, $SrCuO_2$, Pr_6O_{11}, CeO_2, and Cu_2O in adequate molar ratios ($2/2/\frac{1}{6}/1/\frac{1}{2}$) mixed in wet medium (ethanol) using an agate planetar mill. The mixture was then dried, ground and pressed in the form of 1-g pellets. The latter were calcined in a nitrogen flow containing 1% O_2, for 45 hr at 900°C, with a heating rate of 3.8°C min^{-1}, and a cooling rate of 40°C min^{-1}. At this stage, the thermogravimetric analysis indicates that there exists an excess oxygen with respect to the "O_{10}" composition. Thus, the samples were annealed in an argon flow at 725°C, with a heating rate of 100°C hr^{-1} and cooling rate of 30°C hr^{-1}, until no weight loss was observed. The iodometric analysis revealed the composition $Pb_2Sr_2PrCeCu_3O_{9.94}$, showing that, in the limit of the error, this phase corresponds to the reduced form, $\delta = 0$, of the oxide $Pb_2Sr_2PrCeCu_3O_{10+\delta}$.

The X-ray diffraction (X.R.D.) patterns were registered on a Philips vertical diffractometer equipped with a back face monochromator for CuK_α radiation in the range $6° \leq 2\theta \leq 120°$. The neutron diffraction (N.D.) data were registered on D_2B at the ILL facility ($\lambda = 1.5940$ Å) for $5° \leq 2\theta \leq 160°$ with increments of 0.05°. Lattice constants and crystal structure were respectively refined in 12°–120° and 12°–157° 2θ ranges for X.R.D. and N.D. with Rietveld method using a modified version of D.B.W. 3.25 program (*18*).

Electron diffraction (E.D.) was performed with a JEM 120 CX. The high-resolution electron microscopy was carried out with a JEM 200 CX equipped with a top-entry stage using a double tilt goniometer (± 10°) and an objective lens with a spherical aberration constant Cs = 0.8 mm which leads to a theoretical resolution of 0.22 nm. The multislice method of EMS program was used to calculate high-resolution images (*19*).

Results and Discussion

E.D. Study and Cell Parameters

All the crystals exhibit a set of intense reflections corresponding to an orthorhombic cell with an *F* symmetry as shown from the [001] E.D. pattern of Fig. 1a. The X-ray diffractogram of this phase could be indexed, on the basis of this observation, with the following parameters:

$$a = 5.4522\ (2)\ \text{Å},\ b = 5.4807\ (2)\ \text{Å},\ c = 37.012\ (1)\ \text{Å}.$$

Some of the crystals exhibit additional weak reflections besides the fundamental spots. These reflections do not change the parameters, but lead to a variation of the symmetry. Two kinds of lattices have been reconstructed from the E.D. patterns. The first one is illustrated by the [001], [010], and [100] E.D. patterns given in Figs. 1b, 2a, and 2b, respectively; it corresponds to the reflection conditions $h\ k\ l$, $h + l = 2n$ and $h\ 0\ l$, $h, l = 2n$ which are compatible with the space groups *Bmam* and *Bma*2. The second sort of lattice, shown on the [001] E.D. pattern of Fig. 1c, is characterized by the reflection conditions $h\ k\ l$, $h + k = 2n$, $0\ k\ l$, $k, l = 2n$, and $h\ 0\ l$, $h, l = 2n$, compatible with the space groups *Cccm* and *Ccc*2. Note also that both sets of lattices are frequently observed for the same crystal (Fig. 1d).

Moreover, besides these additional reflections, diffuse streaks are also observed, which correspond to an elongation of the intense reflections of the F lattice; such streaks are often oriented along [410]* (Fig. 1a) and more rarely along [110]* (Fig. 1b).

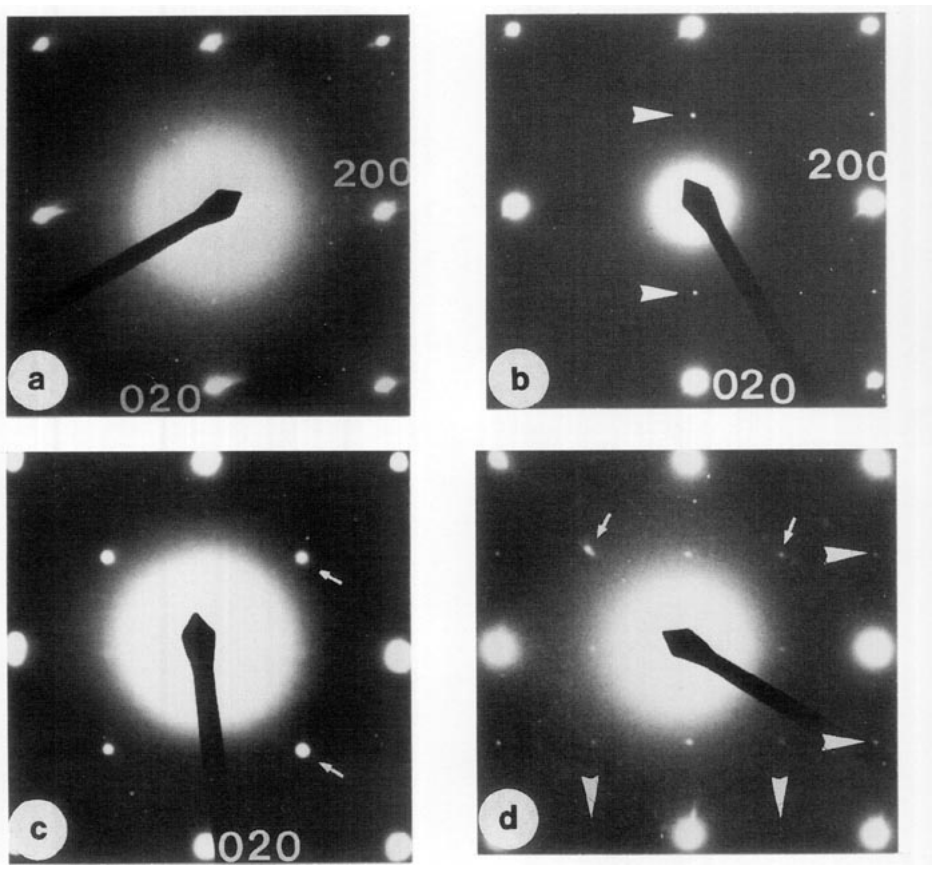

FIG. 1. [001] E.D. patterns showing different existence conditions depending on the microcrystal space group: (a) $h\,k\,0$, ($h = 2n$) ($k = 2n$); s.g. *Fmmm*; (b) $h\,k\,0$, ($h = 2n$); s.g. *Bnam* or *Bma*2; (c) $h\,k\,0$, ($h + k = 2n$); s.g. *Ccm* or *Ccc*2; (d) superposition of (b)-(large arrows) and (c)-type (small arrows) lattices and extra dots due to multiple diffraction.

This phenomenon, which is particularly intense on the F-type crystals, may be due to strains involving a slight monoclinic distortion of the cell.

X.R.D. and N.D. Structure Determination

In order to determine the structure of these phases, the refinements were performed from the X-ray diffraction (X.R.D) and neutron diffraction (N.D) data. The initial variable parameters were deduced from the structural model (Fig. 3) corresponding to a regular intergrowth of the 0201 and 0222 structures, i.e., to the replacement, in the $Pb_2Sr_2YCu_3O_8$ structure, of a $[YO_2]_\infty$ single fluorite layer by a double $[(Pr, Ce)_2O_4]_\infty$ fluorite-type layer.

The refinements were performed from the X-ray data (259 reflections) and from the N.D. data (338 reflections) simultaneously in the space group *Fmmm*. In both cases the profile parameters and structural parameters were refined successively and the impurity phase, $(Pr, Ce)O_2$, was introduced refining its cell parameters and its scale factor in order to subract its contribu-

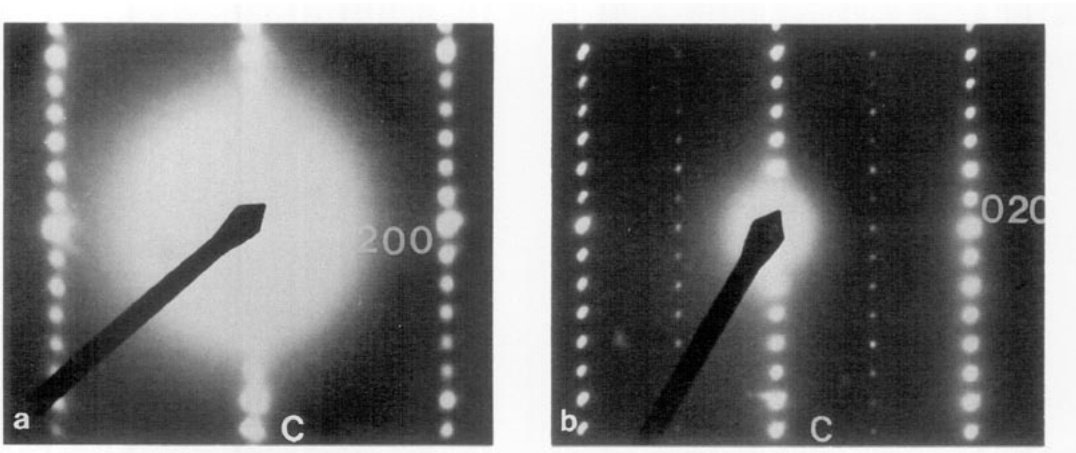

FIG. 2. [010] and [100] E.D. patterns of a *Bmam* (or *Bma2*) microcrystral. (a) $h\ 0\ l$, $h = 2n$ ($l = 2n$); (b) $0\ k\ l$ ($l = 2n$).

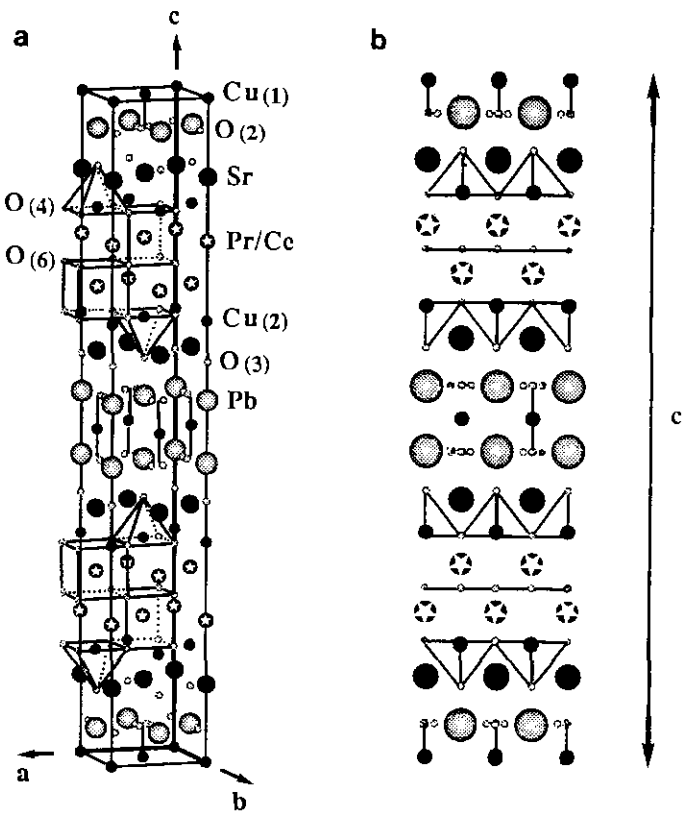

FIG. 3. $Pb_2Sr_2PrCeCu_3O_{10}$ structure: (a) perspective view; (b) [110] projection.

TABLE I

$Pb_2Sr_2PrCeCu_3O_{10}$: STRUCTURAL PARAMETERS, X.R.D. DATA. SPACE GROUP *Fmmm* (*no.* 69), $Z = 4$, $a = 5.4522(2)$ Å, $b = 5.4807(2)$ Å, $c = 37.012(1)$ Å

Atom	Site	x/a	y/b	z/c	B(Å^2)	τ
$Cu_{(1)}$	4*a*	0	0	0	1.2(4)	1.00[b]
Pb	8*i*	1/2	0	0.0474(1)	0.5(1)	1.00[b]
Sr	8*i*	0	0	0.1186(2)	0.3(2)	1.00[b]
$Cu_{(2)}$	8*i*	1/2	0	0.1666(3)	0.1(2)	1.00[b]
Pr/Ce	8*i*	0	0	0.2148(1)	0.1	0.5/0.5[b]
$O_{(1)}$	8*e*	1/4	1/4	0	1[a]	0[a]
$O_{(2)}$[d]	32*p*	0.045(15)	0.077(10)	0.0462(10)	1.0(4)[c]	0.25[a]
$O_{(3)}$	8*i*	1/2	0	0.1054(9)	1.0(4)[c]	1[a]
$O_{(4)}$	16*j*	1/4	1/4	0.1709(8)	1.0(4)[c]	1[a]
$O_{(5)}$	16*j*	1/4	1/4	0.2148	1[a]	0[a]
$O_{(6)}$	8*f*	1/4	1/4	1/4	1.0(4)[c]	1[a]

Profile parameters:
Halfwidth: $u = 0.047(6)$ $\eta = 0.73(1)$
$v = -0.022(6)$
$w = 0.016(1)$

$R_p = 9.9\%$ $R_{wp} = 12.1\%$ $R_{exp} = 7.7\%$ $R_i = 8.0\%$ $R_f = 10.7\%$

[a] Fixed.
[b] Refined prior to fixing.
[c] Simultaneously refined.
[d] Split from 8*i* position [0 0 *z*].

tion though it is quasi-negligible (less than 3%). For X.R.D. calculations, the occupancy factor of the oxygen sites was deduced from N.D. calculations and an overall isotropic B factor was refined for all oxygen atoms. The reliability factors were lowered to the values $R_{wp} = 12.1\%$, $R_{exp} = 7.7\%$, and $R_i = 8.0\%$ for the structural parameters listed in Table I. The N.D. refinements revealcd that the $O_{(2)}$, $O_{(3)}$, $O_{(4)}$, and $O_{(6)}$ sites are fully occupied, whereas the $O_{(1)}$ and $O_{(5)}$ sites located at the level of the $Cu_{(1)}$ sites, and of the *Ln* ions are empty.

The refinement of the B factor of the $O_{(2)}$ site belonging to the $[PbO]_\infty$ layers, i.e., in the 8(*i*) positions for a regular rock salt layer was found abnormally high. For this reason, a splitting of this site in the 32(*p*) positions with an occupancy factor was introduced, which led to a significant improvement of the reliability factors.

The final refinement led to the atomic parameters listed in Table II with the agreement factors $R_{wp} = 9.9\%$, $R_{exp} = 2.9\%$, and $R_i = 8.1\%$. The comparison of the observed and calculated profiles of the N.D. pattern shows that there exist residual peaks on the difference patterns (Fig. 4). All attempts to refine the structure in the groups deduced from the E.D. study, i.e., *Bmam*, *Cccm*, and *Bmab*, did not allow the neutron diffraction profile to be improved, leading to very similar atomic parameters without any significant improvement of the agreement factors. In the same way the refinement of anisotropic thermal factors did not improve

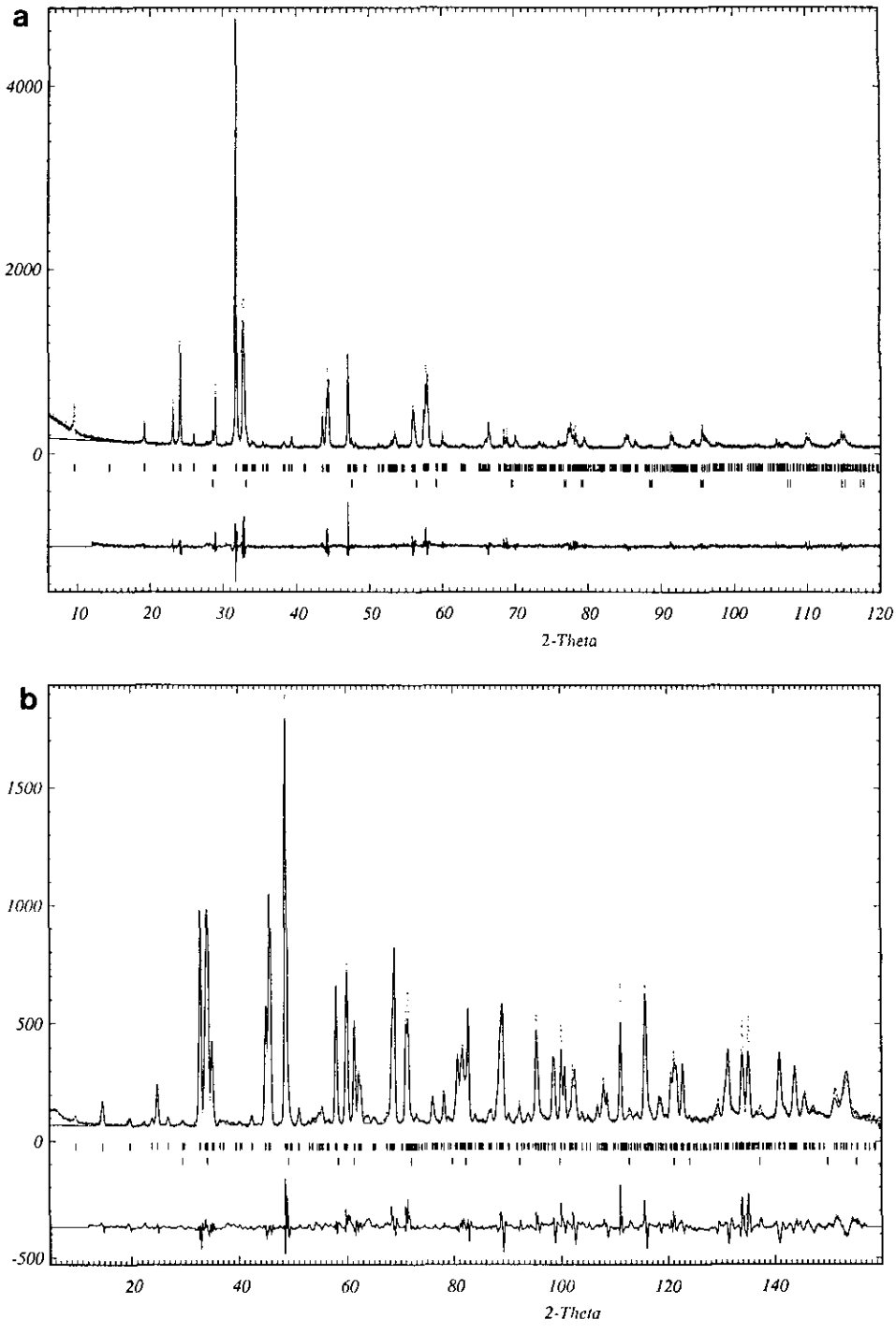

FIG. 4. $Pb_2Sr_2PrCeCu_3O_{10}$ powder patterns: (a) X-ray diffraction; (b) neutron diffraction.

TABLE II

$Pb_2Sr_2PrCeCu_3O_{10}$: STRUCTURAL PARAMETERS, N.D. DATA. SPACE GROUP *Fmmm* (*no.* 69), $Z = 4$, $a = 5.4512(1)$ Å, $b = 5.4799(1)$ Å, $c = 37.0107(8)$ Å

Atom	Site	*x/a*	*y/b*	*z/c*	B(Å^2)	τ
$Cu_{(1)}$	4*a*	0	0	0	1.4(1)	1.01(2)
Pb	8*i*	1/2	0	0.0475(1)	0.91(6)	1.01(1)
Sr	8*i*	0	0	0.1184(1)	1.35(8)	1.01(2)
$Cu_{(2)}$	8*i*	1/2	0	0.1665(1)	0.80(5)	2[b]
Pr/Ce	8*i*	0	0	0.2146(2)	0.31(8)	0.50(1)/0.50(1)
$O_{(1)}$[d]	8*e*	1/4	1/4	0	1[a]	0.02(1)
$O_{(2)}$[c]	32*p*	0.0608(17)	0.0693(15)	0.0491(2)	1.5(2)	0.252(5)
$O_{(3)}$	8*i*	1/2	0	0.1050(2)	1.44(8)	1.00[b]
$O_{(4)}$	16*j*	1/4	1/4	0.1717(1)	1.13(5)	1.00[b]
$O_{(5)}$[d]	16*j*	1/4	1/4	0.2146	1[a]	0.00[b]
$O_{(6)}$	8*f*	1/4	1/4	1/4	0.98(7)	1.00[b]

Profile parameters:
Halfwidth: $u = 0.092(4)$ $\eta = 0.14(1)$
$v = -0.17(1)$
$w = 0.235(5)$

$R_p = 7.8\%$ $R_{wp} = 9.9\%$ $R_{exp} = 2.9\%$ $R_i = 8.1\%$ $R_f = 7.6\%$

[a] Fixed.
[b] Refined prior to fixing.
[c] Split from 8*i* position [0 0 z].
[d] Empty sites at $Cu_{(1)}$ and Pr/Ce level.

the reliability factors. These residual peaks may be due to the existence of strains leading to monoclinic distortion and inhomogeneity as shown from the E.D. study. Taking into account the size of the cell and the great number of reflections it was not reasonable to undertake further refinements in lower symmetry space groups.

These results confirm that the structure of $Pb_2Sr_2PrCeCu_3O_{10}$, consists of a regular intergrowth of the 0201 and 0222 structures, i.e., that it derives from $Pb_2Sr_2YCu_3O_8$ by replacing the $[YO_2]_\infty$ single fluorite-type layer by a $[(Pr, Ce)_2O_4]$ double fluorite-type layer. The atomic coordinates of oxygens deduced from X.R.D. data are, of course, not meaningful, whereas one notes that the variable parameters of the metallic atoms are very similar in both X.R.D. and N.D. studies.

The N.D. study confirms also the "O_{10}" stoichiometry of this phase, and shows a disordered distribution of the oxygen atoms in the $[PbO]_\infty$ layers, traduced by a splitting of the $O_{(2)}$ sites (Fig. 5). It results that lead exhibits three close oxygen neighbors at distances ranging from 2.13 to 2.42 Å (Table III), whereas the two other oxygens are far away (3.08–3.14 Å). In fact, Pb is off-center outside of this "O_5" pyramid, so that its coordination can be better described as tetrahedral (Fig. 6); the PbO_3L tetrahedra consist of three oxygen atoms and of the 6 s^2 lone pair of Pb(II) which is directed in the opposite direction to the oxygen triangle i.e., towards the $Cu_{(1)}$ layer where oxygen atoms are missing (Fig. 6). Such a coordination of lead has previously been observed for $Pb_2Sr_2YCu_3O_8$ (*16*, *17*), $Pb_2Ba_2YCu_3O_8$ (*20*), $PbBaYSrCu_3O_7$ (*21*),

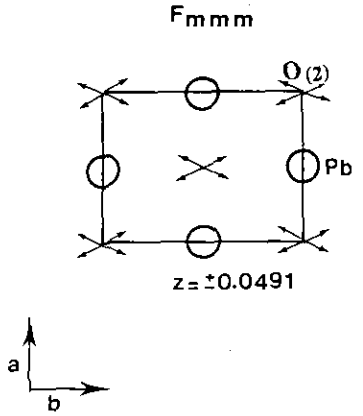

FIG. 5. [001] projection of PbO layer showing the splitted sites of $O_{(2)}$ atom in the *Fmmm* space group.

TABLE III

$Pb_2Sr_2PrCeCu_3O_{10}$: BOND LENGTHS (Å), N.D. DATA

$Cu_{(1)}-O_{(2)}$: 1.886(7) [×2]	$Cu_{(2)}-O_{(3)}$: 2.276(8) [×1]
	$-\ O_{(4)}$: 1.942(1) [×4]
Pb $-\ O_{(3)}$: 2.128(8) [×1]	
$-\ O_{(2)}$: 2.384(8) [×1]	Ln $-\ O_{(4)}$: 2.501(5) [×4]
2.425(9) [×1]	$-\ O_{(6)}$: 2.335(4) [×4]
3.081(9) [×1]	
3.138(8) [×1]	Bond Angles $O-Cu^{I}-O$:
Sr $-\ O_{(2)}$: 2.614(8) [×1]	$O_{(2)}-Cu_{(1)}-O_{(2)}$: 180.0°
$-\ O_{(3)}$: 2.770(1) [×2]	159.8(4)°
2.784(1) [×2]	156.8(3)°
$-\ O_{(4)}$: 2.761(4) [×4]	149.0(4)°

and $PbBa_{0.8}Sr_{1.2}PrCeCu_3O_9$ (*8*). The CuO_5 pyramids exhibit an almost regular basal plane with four equal equatorial Cu–O distances of 1.94 Å, whereas Cu is located at 0.19 Å from this plane, forming an apical Cu–O distance of 2.28 Å (Table III) close to those observed for $Pb_2Sr_2YCu_3O_8$-type oxides. The $Cu_{(1)}$ atom exhibits the twofold coordination with two Cu–O distances of 1.886 Å; note that the existence of mirror plane at the level of $Cu_{(1)}$ does not allow us to determine whether this coordination of copper is linear or not, contrary to what was observed for $PbBaSrYCu_3O_7$ (*21*) and $PbBa_{0.8}Sr_{1.2}PrCeCu_3O_9$ (*8*), for which a O–Cu–O angle of 164° was reported. The LnO_8 cages are slightly elongated along *c* and *Ln* is off-center in its cage, showing a 4 + 4 coordination (Table III); such a tendency of *Ln* to move away from the $[CuO_2]_\infty$ planes towards the intermediate oxygen layer seems to be a characteristic of all cuprates involving double fluorite-type layers.

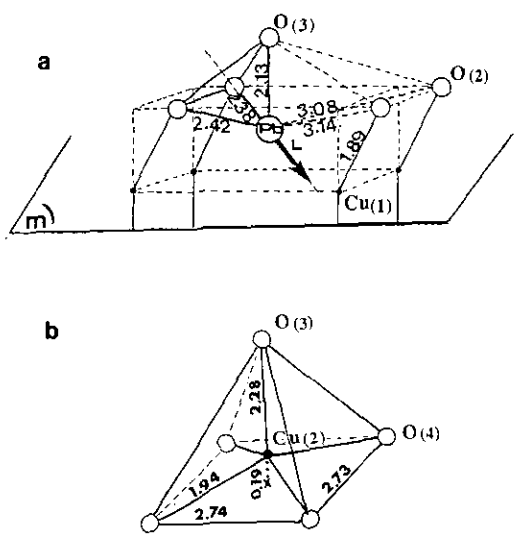

FIG. 6. Perspective view showing (a) Pb atom environment; (b) CuO_5 pyramid.

The valence bond calculations performed from N.D. data confirm that Pb is divalent and the $Cu_{(1)}$ and $Cu_{(2)}$ are univalent and divalent, respectively.

High-Resolution Electron Microscopy Study

As a complement to neutron and X-ray diffraction studies, the microstructural characterization of $Pb_2Sr_2PrCeCu_3O_{10}$ was performed by high-resolution electron microscopy. Twenty-five crystals were characterized, most often with the electron beam parallel to ⟨110⟩, which gives the best description of the atom stacking of the structure (Fig. 3). Most images show a neat contrast which attests of the good crystallinity of the sample and the regular stacking

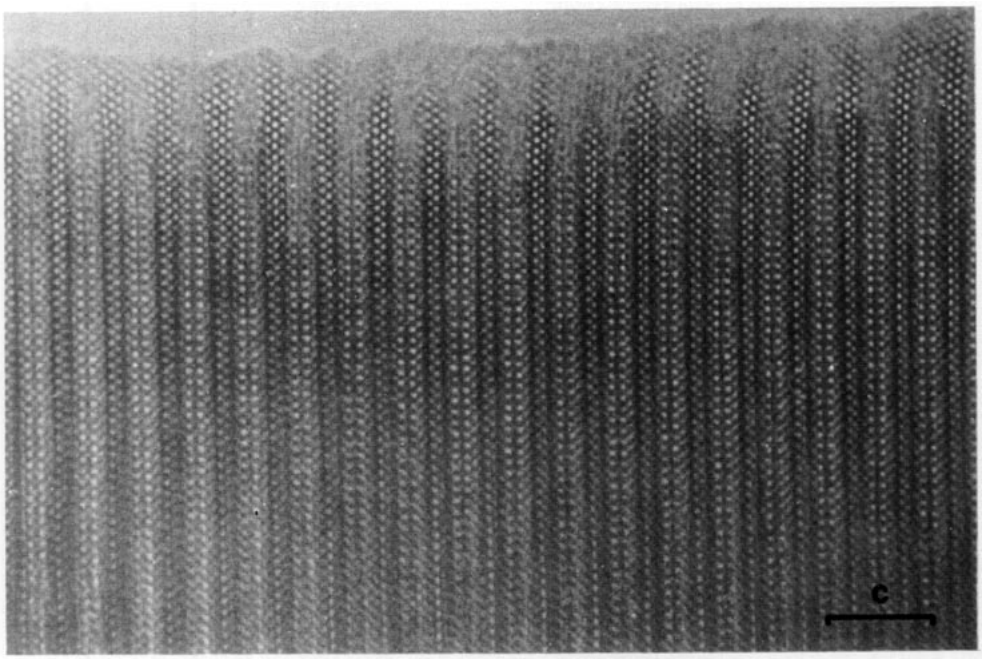

FIG. 7. [110] medium magnification image showing a neat contrast, witness of the sample homogeneity, and the regular stacking of the cations.

of cations of the structure (Fig. 7). In order to confirm high-resolution image interpretation, image calculations have been performed based on neutron diffraction structure resolution results. Figure 8 gives the observed and calculated images of the through-focus series which are the most characteristic of the structure. The 65-nm defocus image gives a good description of cation stacking, where high-electron-den-

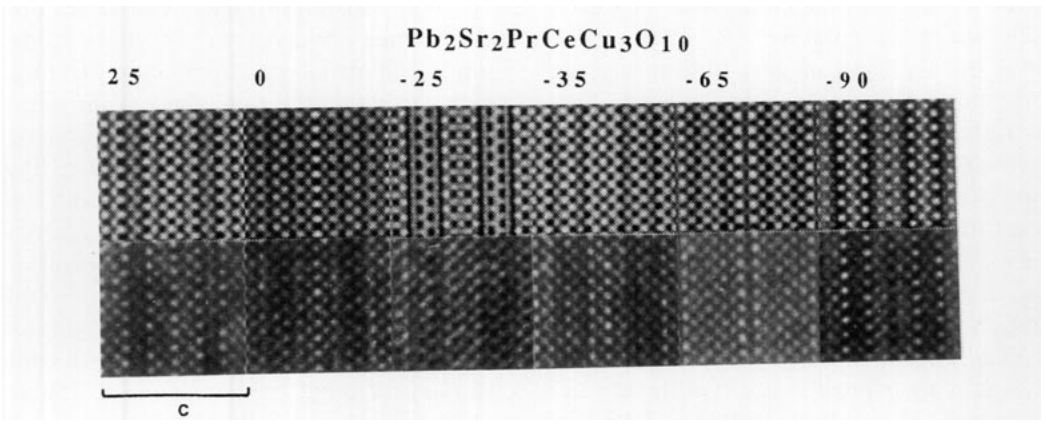

FIG. 8. [110] observed and calculated images. Calculation parameters are: high-voltage $V = 200$ kV, thickness $t = 3.1$ nm, spherical aberration constant Cs = 0.8 mm, defocus spread $\Delta = 12$ nm, convergence semi-angle $\alpha = 0.8$ mrad, defocus is given in nanometer.

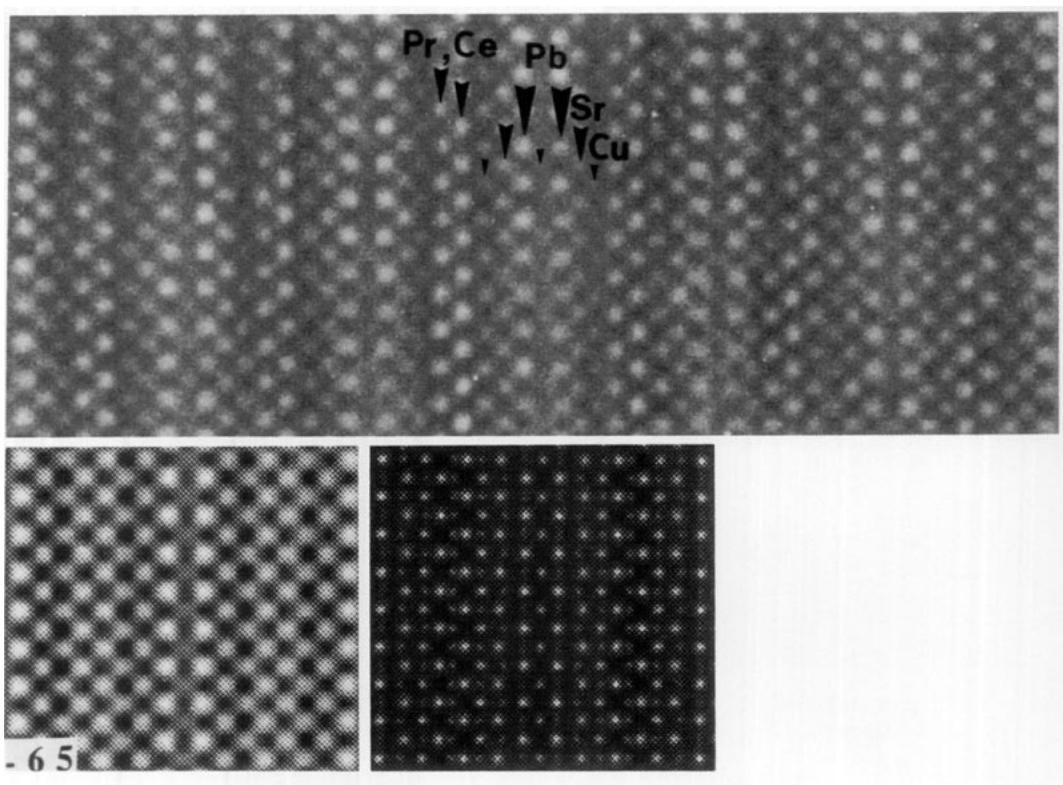

FIG. 9. [110] observed and calculated image for 65-nm defocus and projected potential of $Pb_2Sr_2PrCeCu_3O_{10}$ structure. Dots corresponding to cation sites are arrowed.

sity zones are highlighted (Fig. 9). Brighter dots in two parallel rows can be associated to the Pb cations on either side of $Cu^{I}O_2$ sticks of the structure. Between these rows, the six rows of gray dots in zig zag correspond to the stacking sequence /Sr/Cu/*Ln*/*Ln*/Cu/Sr/. The evenness of the contrast of this image confirms the perfect regularity of the cationic distribution in the structure.

Two features have to be pointed out. The first one deals with stacking faults which have been observed only twice. In both cases, the contrast analysis allowed to identify them as triple fluorite-type layers according to the sequence: $[Pr, Ce]_\infty[O_2]_\infty[Pr, Ce]_\infty[O_2]_\infty[Pr, Ce]_\infty$.

The second feature shows the great similarity with oxides such as $PbBa_{0.8}Sr_{1.2}PrCeCu_3O_9$ (*8*) and $Pb_{0.5}Sr_{2.5}(Nd, Ce)_2Cu_2O_9$ (*14*), involving also double fluorite-type layers. Indeed, one observes as for those compounds, fluorite-type areas $[Pr, CeO_2]_\infty$ which extend on the thin edges of the crystals. Details of the enlarged image show that very frequently a bending of the $[(Pr, Ce)O_2]_\infty$ rows takes place, starting from the crystal edge (Fig. 10); moreover the atom stacking between the fluorite-type slabs is often perturbed on the edge, leading to an amorphous-like contrast. The latter phenomenon is rather unusual, since it was not observed for other oxides involving double fluorite-type layers. It can be due to a greater fragility of the layers involving $Cu^{I}O_2$ sticks, i.e., corresponding to the

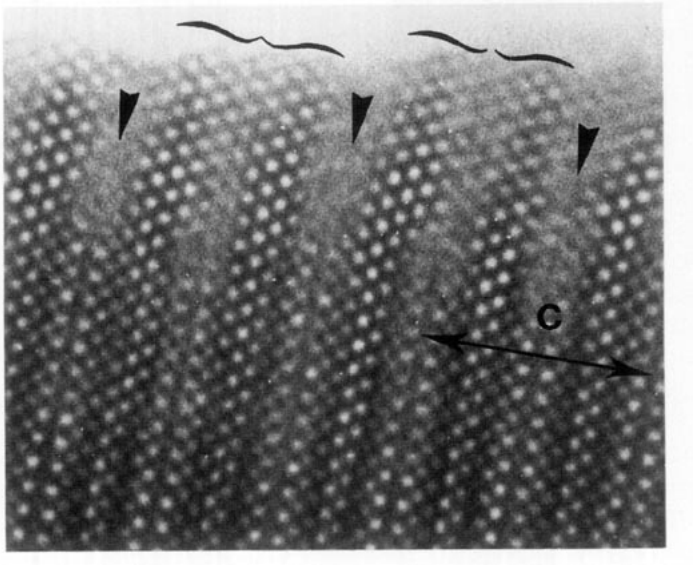

FIG. 10. Detail of a [110] image showing fluorite-type areas on the crystal edge and amorphous areas in-between (arrowed).

stacking "$[PbO]_\infty$–$[Cu]_\infty$–$[PbO]_\infty$." which can be more easily destroyed, when the fluorite layers tend to adapt to the pyramidal copper layers.

Trying to characterize the microstructure of the crystals which show a space group of lower symmetry than *Fmmm*, some crystals with extra spots on their (001) E.D. pattern were selected for high-resolution work. No peculiarity of contrast was detected on the observed images. Nevertheless, an interesting superstructure phenomenon was encountered twice on the ⟨110⟩ images, but very locally. The images of Fig.

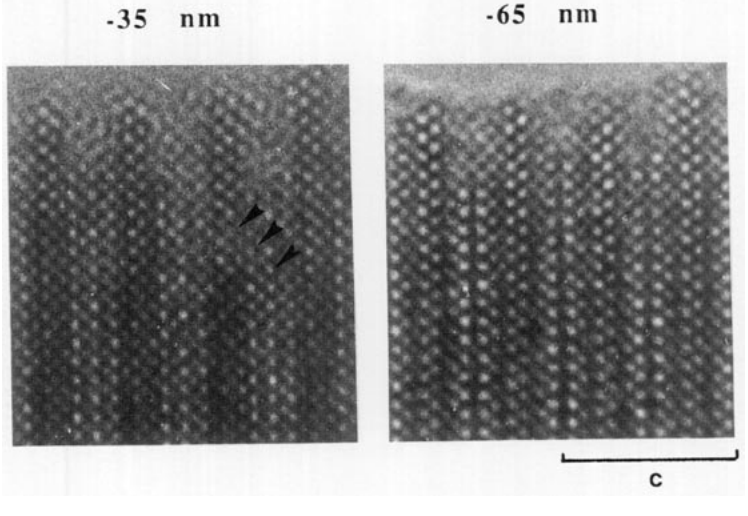

FIG. 11. Detail of a [110] image for two focus values. Very local superstructure is observed on −35-nm image.

11 give details of the same area for two defocus values. On the −35-nm image where low-electron-density areas are highlighted, one row of dots out of two appears brighter, parallel to $[110]_{ReO_3}$. On the −65-nm image, the contrast follows the structure periodicity. This phenomenon, which was confirmed on the through-focus series, suggests a local and ordered variation of oxygen content. It is in good agreement with electron diffraction results. Indeed, a loss of the F symmetry was often detected under the form of very weak extra spots or diffuse streaks on E.D. patterns. As most often H.R.E.M. images shows an even contrast, this could be due to a local rearrangement of the anionic framework, whereas the cationic array follows the regularity of the structure.

References

1. B. Domengès, M. Hervieu, C. Martin, D. Bourgeault, C. Michel, and B. Raveau, *Phase Transitions* **19,** 231 (1989).
2. C. Michel, E. Suard, V. Caignaert, C. Martin, A. Maignan, M. Hervieu, and B. Raveau, *Physica C* **178,** 29 (1991).
3. C. Martin, D. Bourgeault, M. Hervieu, C. Michel, J. Provost, and B. Raveau, *Mod. Phys. Lett. B* **3,** 933 (1989).
4. J. Akimitsu, S. Suzuki, M. Watanabe, and H. Sawa, *Jpn. J. Appl. Phys.* **27,** L1859 (1988).
5. H. Sawa, S. Suzuki, M. Watanabe, J. Akimitsu, M. Matsubara, H. Watabe, S. Uchida, K. Kokusho, H. Asano, F. Izumi, and E. Takayam-Muromachi, *Nature* **337,** 347 (1989).
6. C. Michel, M. Hervieu, and B. Raveau, *J. Solid State Chem.* **92,** 339 (1991).
7. T. Rouillon, D. Groult, M. Hervieu, C. Michel, and B. Raveau, *Physica C* **167,** 107 (1990).
8. T. Rouillon, V. Caignaert, C. Michel, M. Hervieu, D. Groult, and B. Raveau, *J. Solid State Chem.* **97,** 19 (1992).
9. T. Mochiku, T. Nagashima, Y. Saito, M. Watahiki, H. Asano, and Y. Fukai, *Jpn. J. Appl. Phys.* **29,** L588 (1990).
10. R. G. Kulkarni, G. J. Baldha, H. Mohan, R. B. Jotania, H. H. Joshi, V. Skunryev, and K. V. Rao, *Solid State Commun.* **73,** 511 (1990).
11. Y. Tokura, T. Arima, H. Takagi, S. Uchida, T. Ishigaki, H. Asano, R. Beyers, A. I. Nazzal, P. Lacorre, and J. B. Torrance, *Nature* **342,** 890 (1989).
12. H. Sawa, K. Obara, J. Akimitsu, Y. Matsui, and S. Horiuchi, *J. Phys. Soc. Jpn.* **58,** 2252 (1989).
13. T. Wada, A. Ichinose, Y. Yaegashi, H. Yamaushi, and S. Tanaka, *Phys. Rev. B* **41,** 1984 (1990).
14. M. T. Gambardella, B. Domengès, T. Rouillon, M. Hervieu, and B. Raveau, *Eur. J. Solid State Inorg. Chem.* **28,** 1079 (1991).
15. R. J. Cava, B. Batlogg, J. J. Krajewski, L. W. Rupp, L. F. Schneemeyer, T. Siegrist, R. B. Van Dover, P. Marsh, W. F. Peck, P. K. Gallagher, S. M. Glarum, J. M. Marshall, R. C. Farrow, J. V. Waszscak, R. Hull, and P. Trevor, *Nature* **336,** 211 (1988).
16. E. A. Hewat, J. J. Capponi, J. C. Cava, C. Chailloux, M. Marezio, and J. L. Tholence, *Physica C* **157,** 509 (1989).
17. R. J. Cava, M. Marezio, J. J. Krajewski, W. F. Peck, Jr., A. Santoro, and F. Beech, *Physica C* **157,** 272 (1989).
18. D. B. Wiles and R. A. Young, *J. Appl. Crystallogr.* **14,** 149 (1981).
19. P. A. Stadelmann, *Ulramicroscopy* **21,** 131 (1987).
20. W. T. Fu, H. W. Zandbergen, W. G. Haije, and L. J. De Jongh, *Physica C* **159,** 210 (1989).
21. T. Rouillon, V. Caignaert, M. Hervieu, C. Michel, D. Groult, and B. Raveau, *J. Solid State Chem.* **97,** 56 (1992).